Chapter 6

Correlations in a coupled quantum-dot molecule

In the two previous Chapters I have discussed the manifestations of correlations in a system of N electrons confined by a parabolic quantum dot. In this Chapter I shall move on to considering correlation effects in more complicated systems, composed of electrons and holes confined in self-assembled quantum dots.

My approach to the electronic systems involved distributing the electrons on the single-particle levels of the parabolic potential and analysing how the configurations thus created are coupled by Coulomb interactions of the carriers. I demonstrated that the strength of interactions relative to characteristic single-particle energies could be tuned by changing either the confinement energy Ω_0 or the external magnetic field. Such tuning is more difficult in the case of SADs. In Section 2.2 I have shown that for these structures the orbital energy quantisation is so strong that even the magnetic fields of magnitudes of order of 10 T modify the spectra only slightly. The only way of influencing the ratio of single-particle orbital to interaction energies is thus the manipulation of the QD confinement. In this Chapter I shall move from weakly to strongly interacting systems not by changing Ω_0 of

a single QD, but by changing the separation between two coupled quantum disks.

A schematic diagram of the system of two vertically coupled quantum disks is presented in Fig. 6.1 (a). The disks have the same height H and are horizontally aligned in such a way that they share the axis of rotational symmetry. The disk radii are denoted as R_1 (bottom disk) and R_2 (top disk); in general, $R_1 \neq R_2$. Each disk is formed on a thin wetting layer, and the thickness of the tunnelling barrier between disks is controlled by the distance D between these layers. The quantum-mechanical coupling between the two dots leads to formation of quantum-dot molecular orbitals analogous to those found in diatomic molecules. Energies corresponding to these orbitals are sensitive to the distance between dots, and therefore by tuning the distance D one can tune the single-particle energy spectrum of the system.

6.1 Single-particle states of the QD molecule

Before I can consider the system of many particles confined in the double-dot molecule, I first have to analyse its single-particle energy spectrum. This analysis is presented in the paper "Electronic structure of vertically stacked self-assembled quantum disks", published by M. Korkusiński and P. Hawrylak in Physical Review B, vol. 63, page 195311 (2001). This publication is an integral part of this thesis and is appended to the presented material. Here I shall summarise its most important points.

Let us start with a simple model of a single electron confined by the molecule composed of two identical disks. Let us also assume that the single-particle energy spectrum of each individual disk consists of a single orbital, whose energy will be denoted as E_s. Since the disks are identical, the energy E_s of the top disk is equal to that of the bottom disk. In the absence of interdisk tunnelling, the electron can occupy either the bottom disk (say, disk 0) or the top disk (disk 1). Its state can therefore be labelled by the quantum-dot layer index, or isospin: $|0\rangle$ or $|1\rangle$.

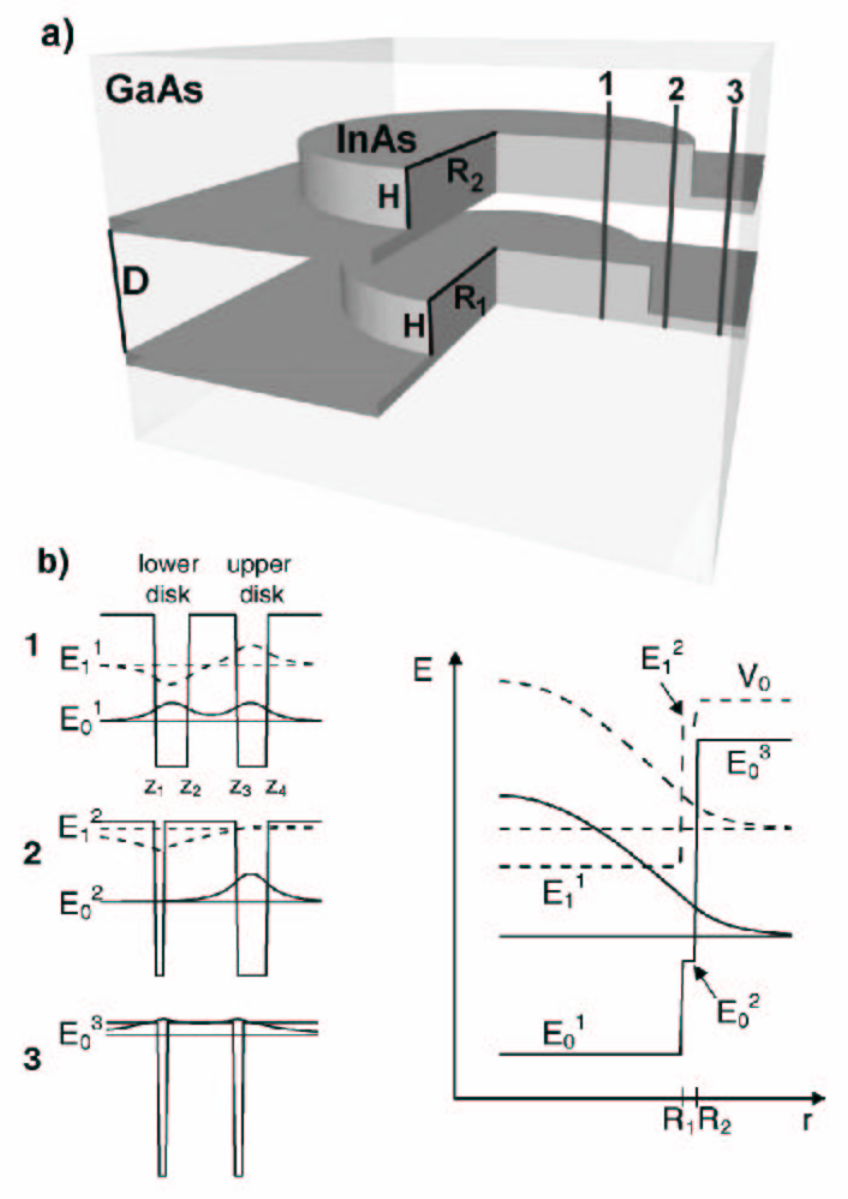

Figure 6.1: (a) Schematic picture of the vertically coupled double-dot molecule; (b) illustration of effective potentials in the adiabatic calculation of electronic states for the vertical motion (left-hand panel) and for the planar motion (right-hand panel) (see text for details)

Let us now include the tunnelling. The Hamiltonian of this simple double-dot molecule written in the basis of the isospin states takes the form

$$\hat{H} = \sum_{i=0}^{1} E_s c_i^+ c_i - t(c_0^+ c_1 + c_1^+ c_0), \tag{6.1}$$

or, in a matrix form,

$$H = \begin{bmatrix} E_s & -t \\ -t & E_s \end{bmatrix}. \tag{6.2}$$

Diagonalisation of this simple matrix yields the molecular eigenstates and eigenenergies: the symmetric (or bonding) orbital $|+\rangle = \frac{1}{\sqrt{2}}(|0\rangle + |1\rangle)$ with energy $E_+ = E_s - t$, and the antisymmetric (or antibonding) orbital $|-\rangle = \frac{1}{\sqrt{2}}(|0\rangle - |1\rangle)$ with energy $E_+ = E_s + t$. These energy levels are split by $2t$, and the value of this splitting depends on the thickness of the tunnelling barrier between disks, measured by the QD layer distance D. If D is large, the tunnelling matrix element t is small, and the two molecular orbitals are nearly degenerate. On the other hand, if D is decreased, then the splitting between the energies $E_\pm$ increases.

Let us now present a more realistic calculation for a pair of coupled self-assembled InAs quantum disks embedded in the GaAs barrier material. The calculation is done within the effective mass approximation. The single-particle Hamiltonian of the system, written in cylindrical coordinates and in the effective units of energy and length (Section 2.2) takes the form:

$$\hat{H} = -\frac{1}{r^2}\left(r\frac{\partial}{\partial r}r\frac{\partial}{\partial r} + \frac{\partial^2}{\partial \theta^2}\right) - \frac{\partial^2}{\partial z^2} + V(r,z), \tag{6.3}$$

where $V(r,z)$ is the double-disk potential.

In Sections 2.2 and 2.3 I have considered similar Hamiltonians, with the quantum disk and quantum ring confinement potentials, and I assumed that these potentials have barriers of infinite height. In the case of the quantum disk this assumption led to the separation of the Hamiltonian into two operators: one describing the vertical motion, and the other - the lateral motion of the particle. The two resulting Schrödinger equations could be then solved analytically.

But in order to account for the quantum-mechanical coupling in my double-disk system I need to consider a potential $V(r,z)$ whose walls are of finite height. This complicates the analysis in that now the Hamiltonian (6.3) is not separable into two operators, and the corresponding Schrödinger equation cannot be solved analytically even at zero magnetic field. To gain insight into the properties of the single-particle spectrum of the double-disk potential without resorting to numerical treatment, we have proposed a semi-analytical adiabatic approximation, involving an artificial separation of the motion in z direction from the motion in the plane. This method is fast and portable, and allows to obtain energies and wave functions of bound states as a function of the distance between disks with minimal computational effort even if the disks are not identical (they can vary both in width and radius).

In the adiabatic approximation the electronic wave functions are sought in the following form:

$$\psi(r,\theta,z) = \frac{1}{\sqrt{2\pi}} e^{im\theta} \times g_r^\nu(z) \times f_m^\nu(r). \tag{6.4}$$

The first term in this formula is the angular wave function. Isolating it from the rest of the total wave function is not an approximation, since the system is rotationally symmetric, and all electronic orbitals have a well-defined angular momentum m. The approximate character of the method lies in writing the rest of the wave function ψ in the form of a product of the function g dependent on the z coordinate and the function f dependent on the radial coordinate. The Schrödinger equation constructed with the Hamiltonian (6.3) and the wave function as above can be formally separated into two coupled equations:

$$\left[-\frac{\partial^2}{\partial z^2} + V(r,z)\right] g_r^\nu(z) = E_\nu g_r^\nu(z), \tag{6.5}$$

$$\left[-\frac{1}{r^2}\left(r\frac{\partial}{\partial r} r \frac{\partial}{\partial r} - m^2\right)\right] f_m^\nu(r) = (E - E_\nu(r)) f_m^\nu(r). \tag{6.6}$$

Let us now describe how the two equations were solved.

The equation (6.5) is solved first. It describes the vertical motion of an electron in the potential $V(r,z)$ for a given value of the radial coordinate r. In Figure 6.1 (a) and (b) I

show that, depending on the coordinate r, one deals with three different potentials $V(r,z)$: if $r < R_1$ I have two wide quantum wells, each of width equal to the height H of the disk plus the width W of the wetting layer; if $R_1 < r < R_2$ I have one wide well, corresponding to the top disk, and one narrow well, corresponding to the wetting layer, and finally for $r > R_2$ I have a double-well structure composed of the two wetting layers. I solve for the motion of the electron in each of these cases using the transfer-matrix method, described in detail in the paper. For further analysis I retain two lowest energies, $E_\nu = E_0$ and $E_\nu = E_1$ and the two corresponding orbitals g^0 and g^1. The energy E_0 is the energy of the symmetric solution, corresponding to the bonding quantum-molecular orbital, and the energy E_1 is the antisymmetric solution, corresponding to the antibonding quantum-molecular orbital. The corresponding wave functions in each radial region are drawn in the left-hand panel of Fig. 6.1 (b). Their symmetric and antisymmetric character is apparent in the first region, where the confining potential is a pair of identical quantum wells. In the second region the potential is no longer symmetric, and therefore here the bonding and antibonding orbitals do not have a definite symmetry. This symmetry is restored in the third region, when I again deal with two identical quantum wells. However here the wells are narrow, and only the bonding orbital is confined.

The energies E_ν are different in each region. Out of them I build the effective potential $E_\nu(r)$ for the lateral motion of the electron, which is illustrated in the right-hand panel of Fig. 6.1(b). This effective potential is built for each subband ν separately and inserted into the equation (6.6). The radial equation for each subband is solved using the transfer-matrix method, presented in detail in the paper. The energies E obtained as a result of the calculation form the single-particle spectrum of the system.

The adiabatic effective-mass approximation requires two parameters as input: the effective mass m^* of the carrier and the depth V_0 of the confining potential $V(r,z)$. They determine how many bound states there are in the single-particle spectrum, and how sensitive this spectrum is to the change of the interdisk distance. Thus I need to establish

the parameters m^* and V_0 for existing double-dot systems.

In Chapter 1 I have described the techniques of fabrication of stacked InAs disks embedded in the GaAs barrier material. The depth of confinement V_0 in such systems is determined by the alignment of band edges of the constituent materials. If the bulk properties of GaAs and InAs is used, the conduction band edge of the dot material is about 1 eV below the conduction band edge of the barrier, and the confinement in the degenerate heavy- and light-hole subbands of the valence band is of order of 85 meV. However, strain present in the system modifies these confinement depths dramatically: the confinement of electrons is in reality of order of 600 meV. Moreover, the hole subbands are split, the heavy-hole confinement is enhanced, and the light-hole confinement is decreased. The strain-induced modifications to the confinement potential can be calculated using the Bir-Pikus formalism [21]. I will show the results of such calculations below.

The effective mass m^* of the carriers is also influenced by the strain, but in the framework of the effective mass approximation we are not able to assess this influence quantitatively. Therefore the effective mass is treated as the fitting parameter in the electronic calculations, and it can be adjusted to obtain agreement with more sophisticated microscopic calculations or with the experiment.

Let us now demonstrate how the presence of strain can be accounted for in the calculations of electronic structure of the system. This discussion is presented briefly in the paper; here I shall provide some supplementary details [56].

Let us start by calculating the distribution of strain in my system. The strain is due to the mismatch of lattice constants of the dot and barrier materials; in this InAs/GaAs system this mismatch is of order of 7%. The degree of strain is quantitatively described with strain tensor matrix elements

$$\varepsilon_{ij}(\mathbf{r}) = \frac{1}{2}\left(\frac{\partial u_i(\mathbf{r})}{\partial x_j} + \frac{\partial u_j(\mathbf{r})}{\partial x_i}\right), \tag{6.7}$$

where $\mathbf{u}(\mathbf{r})$ is a vector describing the displacement of a small element of the system at coordinate $\mathbf{r}$ from its equilibrium position. The distribution of these strain elements in

this system can be calculated using several methods (for reviews see Refs. [56, 99]). I use the continuous elasticity theory, in which the total elastic energy of the system is written as

$$\begin{aligned} E &= \int d^3r \left\{ \frac{1}{2} C_{11}(\mathbf{r})(\varepsilon_{xx}^2 + \varepsilon_{yy}^2 \varepsilon_{zz}^2) + C_{12}(\mathbf{r})(\varepsilon_{xx}\varepsilon_{yy} + \varepsilon_{xx}\varepsilon_{zz} + \varepsilon_{yy}\varepsilon_{zz}) \right. \\ &+ \left. 2C_{44}(\varepsilon_{xy}^2 + \varepsilon_{xz}^2 \varepsilon_{yz}^2) - \alpha\varepsilon_0(\varepsilon_{xx} + \varepsilon_{yy} + \varepsilon_{zz}) \right\}. \end{aligned} \tag{6.8}$$

Here C_{11}, C_{12}, and C_{44} are the material-specific elastic constants, and $\varepsilon_0 = (a_{dot} - a_{barrier})/a_{barrier}$ is the relative difference between the lattice constants a of the dot and the barrier, respectively. The parameter $\alpha = C_{11} + 2C_{12}$ in the dot material, and zero in the barrier. The calculation of strain distribution involves discretising the system on a grid of points and minimising the above total elastic energy with respect to displacements of grid nodes $\mathbf{u}(\mathbf{r})$. In the paper (Figure 3 (a), (b), (c), and (d)), I show, respectively, the distributions of the strain matrix elements ε_{xx}, ε_{yy}, ε_{zz}, and the hydrostatic strain $\varepsilon_h = \varepsilon_{xx} + \varepsilon_{yy} + \varepsilon_{zz}$ on the vertical plane through the centre of both disks assuming the disk radii $R_1 = 8$ nm, $R_2 = 8.5$ nm, disk thicknesses $H = 2$ nm and the QD layer distance $D = 4$ nm. To supplement this presentation, I show again the distribution of the hydrostatic strain $\varepsilon_h = \varepsilon_{xx} + \varepsilon_{yy} + \varepsilon_{zz}$ and the biaxial strain $\varepsilon_B = \varepsilon_{zz} - \frac{1}{2}(\varepsilon_{xx} + \varepsilon_{yy})$ in Figure 6.2 (a) and (b), respectively. From Fig. 6.2 one can see that as we move along the symmetry axis through the centre of both disks, the hydrostatic strain remains negative (compressive) throughout, but the sign of the biaxial strain changes on the dot-barrier interfaces: it is positive inside the disks and negative in the barrier.

As the unit cell of the crystal is deformed by strain, the bond lengths and angles change, and this in turn influences the band structure. The attempt to describe this effect within the $\vec{k} \cdot \vec{p}$ formalism was undertaken by Bir and Pikus [21] for the diamond-type lattices. Bahder [12] extended their approach to the zinc-blende binary semiconductor alloys using

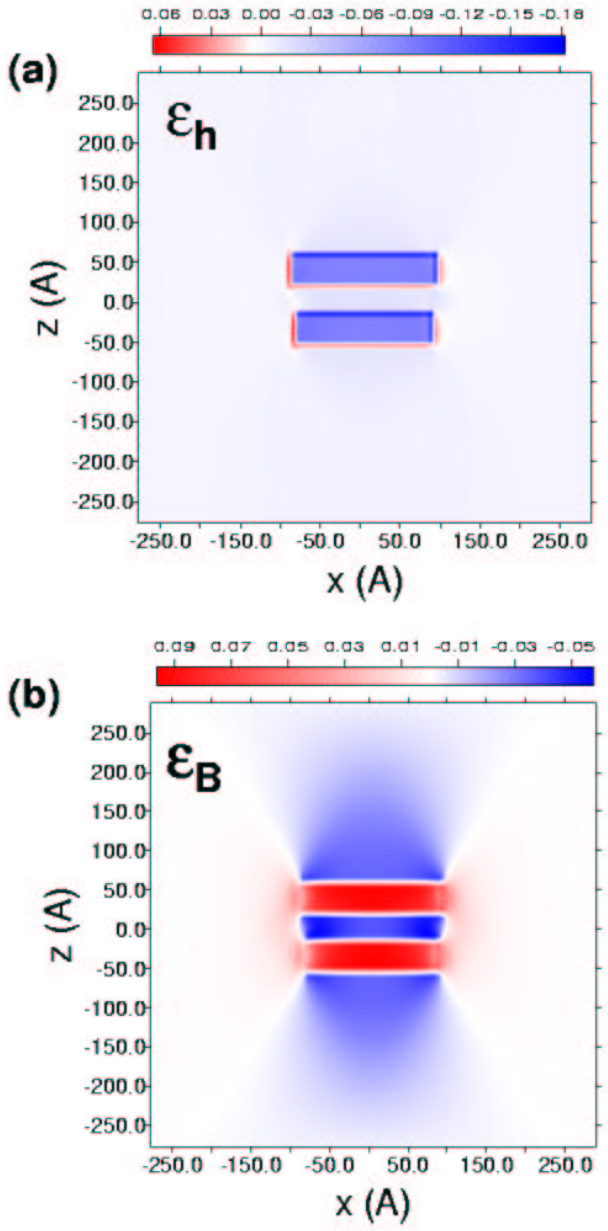

Figure 6.2: Vertical cross section of the spatial variation of hydrostatic (a) and biaxial (b) strain components through the centre of the double-disk InAs/GaAs system

the Löwdin perturbation theory and obtained the following eight-band $\vec{k}\cdot\vec{p}$ Hamiltonian:

$$\hat{H}_{\text{strain}} = \begin{pmatrix} a_c\varepsilon_h & 0 & -v^* & 0 & -\sqrt{3}v & \sqrt{2}u & u & -\sqrt{2}v^* \\ 0 & a_c\varepsilon_h & \sqrt{2}u & \sqrt{3}v^* & 0 & v & -\sqrt{2}v & -u \\ -v & \sqrt{2}u & -p+q & -s^* & r & 0 & \sqrt{3/2}s & -\sqrt{2}q \\ 0 & \sqrt{3}v & -s & -p-q & 0 & r & -\sqrt{2}r & \sqrt{1/2}s \\ -\sqrt{3}v^* & 0 & r^* & 0 & -p-q & s^* & \sqrt{1/2}s^* & \sqrt{2}r^* \\ \sqrt{2}u & v^* & 0 & r^* & s & -p+q & \sqrt{2}q & \sqrt{3/2}s^* \\ u & -\sqrt{2}v^* & \sqrt{3/2}s^* & -\sqrt{2}r^* & \sqrt{1/2}s & \sqrt{2}q & -a_v\varepsilon_h & 0 \\ -\sqrt{2}v & -u & -\sqrt{2}q & \sqrt{1/2}s^* & \sqrt{2}r & \sqrt{3/2}s & 0 & -a_v\varepsilon_h \end{pmatrix}, \tag{6.9}$$

where

$$\begin{aligned} p &= a_v\varepsilon_h, \\ q &= b\left[\varepsilon_{zz} - \frac{1}{2}(\varepsilon_{xx}+\varepsilon_{yy})\right], \\ r &= \frac{\sqrt{3}}{2}b(\varepsilon_{xx}-\varepsilon_{yy}) - id\varepsilon_{xy}, \\ s &= -d(\varepsilon_{xz}-i\varepsilon_{yz}), \\ u &= -\frac{i}{\sqrt{3}}P_0\sum_j \varepsilon_{zj}\partial_j, \\ v &= = -\frac{i}{\sqrt{6}}P_0\sum_j (\varepsilon_{xj}-i\varepsilon_{yj})\partial_j, \end{aligned} \tag{6.10}$$

with the parameters a_c, a_v, b and d being the material-dependent deformation potentials, and P_0 being the imaginary valence-conduction band coupling.

The above formula is written in the notation of Pryor *et al.* [99]. I can use it to calculate the local band edge profiles at each point of the grid used previously in the strain calculations. To this end, however, one can set the parameters u and v to zero, as I am only interested in the band structure at the Γ point of the Brillouin zone. Then, from Eq. (6.9) one can easily see that the conduction band is not coupled to the valence band, and that the strain-induced modification of the conduction band edge consists only of a shift proportional to the hydrostatic strain. The valence band, on the other hand, is

much more complicated. I will focus here mainly on understanding the diagonal elements of the matrix H_{strain}. It can be readily seen that all heavy- and light-hole band edges are shifted by $-p$, which is proportional to the hydrostatic strain. Further, the strain introduces a splitting between the heavy and light hole band edges equal to $2q$, if the off-diagonal elements are disregarded. As can be seen from Eq. (6.10), the parameter q is proportional to the biaxial strain, and depends on the deformation potential b, which is negative for most semiconductors. That means that if the biaxial strain is negative (compressive), the heavy hole band edge will lie above the light hole band edge (i.e., from the viewpoint of the holes, the heavy hole band will have a lower energy). If the biaxial strain is positive, the situation is reversed.

Now I input the calculated distributions of strain tensor matrix elements into the Bir-Pikus Hamiltonian (6.9) and, for each point of the structure, diagonalise it numerically to obtain the strain-modified profiles of band edges. The result of these calculations is shown in Fig. 6.3. This figure is similar to the Figure 4 from the paper and differs only in the valence band. Figure 6.3 indicates that the edge of the heavy-hole subband (green line) crosses the edge of the light-hole subband (blue line) at all dot-barrier interfaces. This is the correct picture; the assignment of bands in Figure 4 from the paper is erroneous. The crossing of light-hole and heavy-hole band edges is due to the fact that the biaxial strain changes sign at the barrier dot interfaces. Since the biaxial strain controls the splitting between the heavy- and light-hole bands, the change of sign of this strain component leads to the reversal of bands. This effect has also been reported, e.g., in Ref. [112].

The strain calculations coupled to the Bir-Pikus formalism suggest that the parameter V_0 in my InAs/GaAs system is reduced to 600 meV. Using this confinement depth and treating the effective mass m^* as a fitting parameter, the electronic spectra were fitted to those obtained with a similar system within the eight-band $\vec{k} \cdot \vec{p}$ formalism. As a result of this fitting, the electronic effective mass was found to be $m^* = 0.053\ m_0$.

With the adiabatic effective mass approximation fully defined and parametrised I

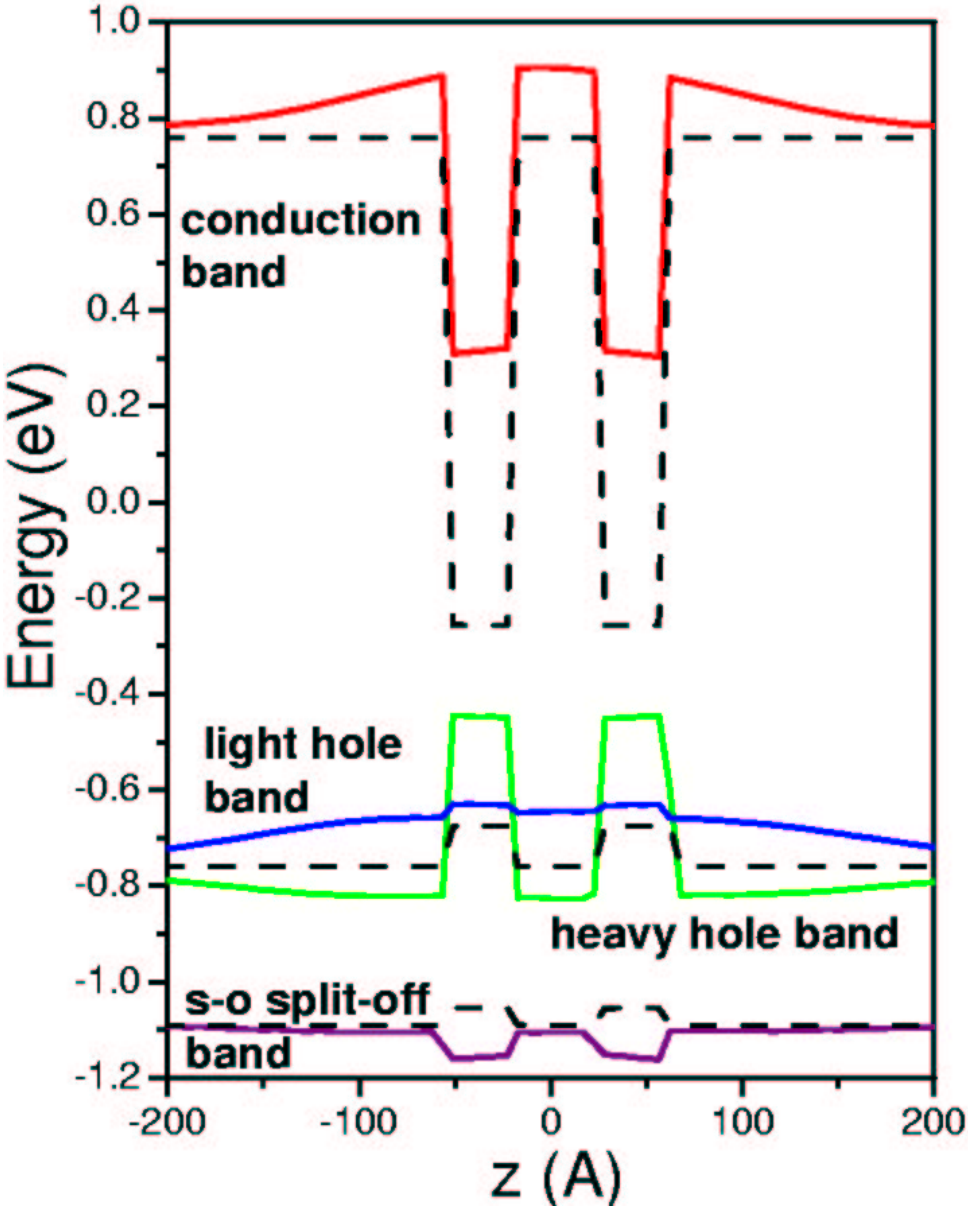

Figure 6.3: Band edge alignment along the symmetry axis of the system (dotted lines - unstrained, solid lines - with strain)

have calculated the electronic spectra of the vertically coupled double-disk InAs/GaAs molecule. The spectrum for the double-disk structure with radii of $R_1 = 8$ nm, $R_2 = 8.5$ nm and height of each disk of $H = 2$ nm is shown in Fig. 6.4. Due to the finite depth of the confinement potential there are only a few bound electronic states. These states possess a new characteristic property due to the double-dot potential: they are either symmetric or antisymmetric in the direction along the axis of rotational symmetry. These symmetry properties are analogous to those of bonding and antibonding states in diatomic molecules. The energies of these states change as a function of the distance between disks, as shown in Fig. 6.4. At large interdisk distances the symmetric and antisymmetric states associated with the same radial and angular modes (i.e., characterised by the same quantum numbers n and m) are almost degenerate - one deals essentially with two uncoupled quantum disks. Small splittings between these levels are due to the fact that the disks are not identical. Of course, for each vertical symmetry I find the ladder of levels with different quantum numbers n and m, as I did in the case of the single disk in Section 2.2.

As the two disks are shifted closer together, the tunnelling through the interdisk barrier causes the symmetric and antisymmetric states to split. This splitting increases exponentially as the distance between disks is decreased, and can become as large as the energy gap between two adjacent shells of each disk (which is of order of 30 meV), so that a symmetric state of, say, the p shell can become degenerate with the antisymmetric state of the s shell (this situation corresponds to the QD layer distance of 45 Å). Thus I deal with a situation distinctly different from that of the single disk: there, the vertical energy quantisation introduced the largest energy scale of the system; here this energy scale is typically the smallest. For all interdisk distances the ladder of lateral modes built on top of each vertical mode exhibits the shell structure characteristic for the disk confinement (I covered it in detail in Section 2.2).

In the paper we also discuss the case of nonzero magnetic field, however, unlike in Section 2.2 for a single quantum disk, the field is now perpendicular to the axis of rota-

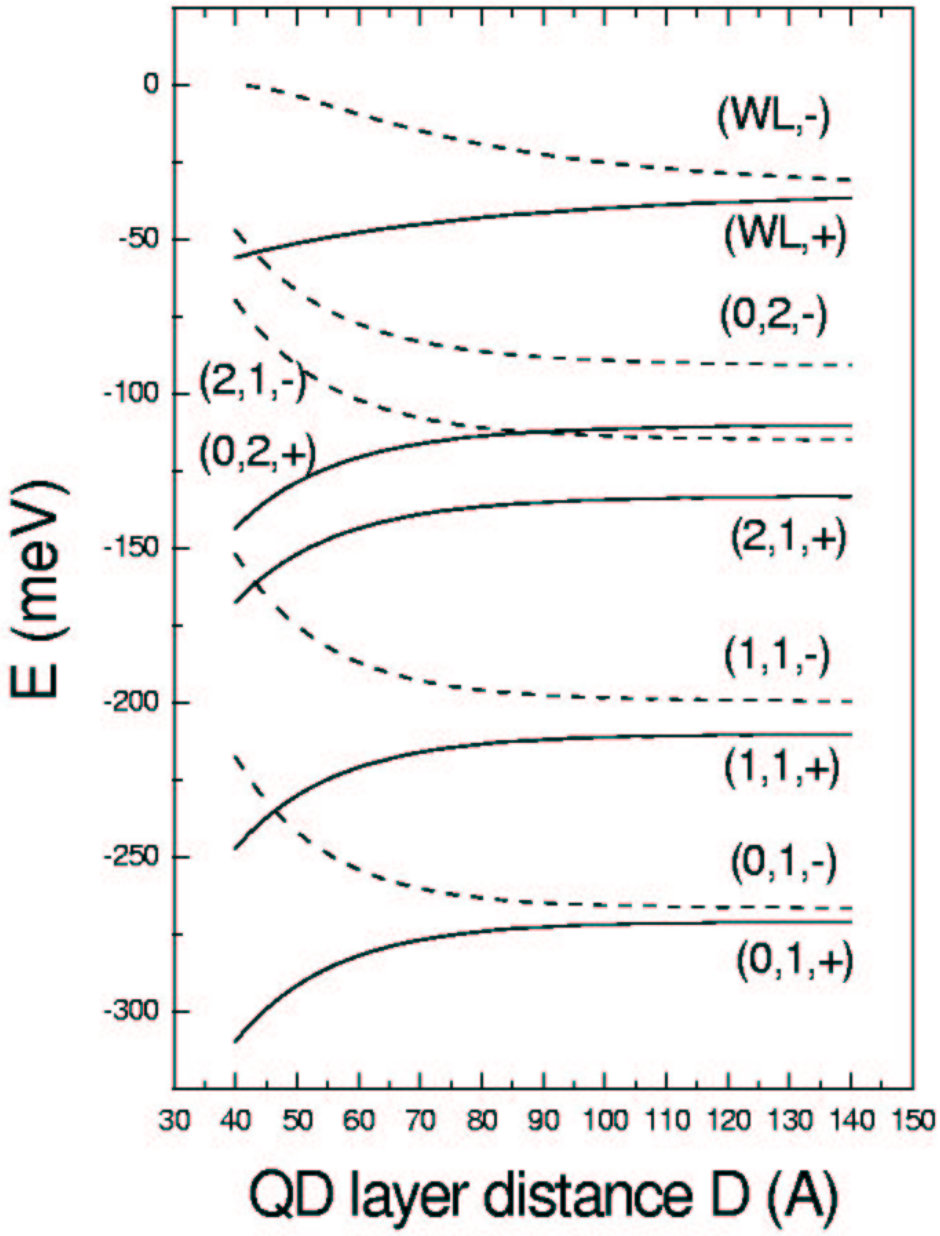

Figure 6.4: Electronic energy levels for a double-disk structure with confinement $V_0 = 600$ meV and electronic effective mass $m^* = 0.053\ m_0$. WL denotes the states of the wetting layer. Numbers in braces denote quantum numbers (n, m, l) of the states. $l = +$ denotes a symmetric state (solid lines), while $l = -$ denotes an antisymmetric state (dashed lines)

tional symmetry. We have chosen this alignment, since, as I have shown in Section 2.2, the magnetic field aligned in parallel to the rotational axis has relatively little effect on the spectrum even at fields of order of 10 T. The second reason is the fact that the magnetic field directed perpendicularly to the rotational axis couples the symmetric and the antisymmetric states, and can lead to anticrossing of shells which originally had opposite symmetries. This is clearly seen in Figure 7 in the paper, where we show this anticrossing behaviour as a function of the interdisk distance e.g., for the antisymmetric s shell and the symmetric p shell (the anticrossing is seen for the distance between disks of 45 Å, i.e., at the point where at zero magnetic field the two states cross).

6.2 Entangled states of an electron-hole complex in the QD molecule

Let us now discuss the properties of a single electron-hole pair confined in the double-disk quantum molecule. I focus on discussing the structure of the states of the electron-hole pair in the context of entanglement, being a special kind of particle-particle correlations.

The results of this work were published in the paper "Entangled states of electron-hole complex in a single InAs/GaAs coupled quantum dot molecule", by Marek Korkusiński, Pawel Hawrylak, Manfred Bayer, Gerhard Ortner, Alfred Forchel, Simon Fafard, and Zbigniew Wasilewski, published in Physica E, vol. 13, page 610 (2002). This publication is an integral part of this thesis and is appended to the presented material.

The notion of entanglement is of particular importance in quantum computing, where the information is stored in quantum bits. Quantum phenomena must be also used to process this information, and the simplest object capable of doing so is the quantum logic gate. The operation of such gate relies on the existence of entangled states of constituent qubits, i.e., states which cannot be obtained by individual qubit rotation. If I were to

change the state of one qubit in the entangled system, I would nontrivially affect the state of the entire system.

In the paper, we have proposed a model of a quantum logic gate composed of two qubits - an electron and a hole - confined in a vertically coupled pair of disk-shaped self-assembled quantum dots. Since we deal with an electron-hole pair - an exciton, such a system can be examined optically - by the photoluminescence experiment. My goal is to predict the luminescence spectra of the exciton and, in these spectra, find features proving the existence of entangled states.

In this simple analysis, I return to my original description of the single-particle molecular orbitals in the language of isospin states, and assume that the two quantum disks are identical. In the absence of the interdisk tunnelling, the particle can be localised either on the bottom disk (isospin state $|0\rangle$) or on the top disk (isospin state $|1\rangle$), and these states are identified as the states of the qubit. Tunnelling through the barrier between disks leads to mixing of isospin states, i.e., rotation of the qubit. One observes the formation of molecular orbitals $|\pm\rangle = \frac{1}{\sqrt{2}}(|0\rangle \pm |1\rangle)$ and their energies $E_\pm$ are split by $2t$. The tunnelling matrix element t is the only free parameter; its value for each interdot distance can be easily established from the single-particle spectra calculated using the adiabatic effective-mass approximation.

Let us now introduce the second qubit - the hole - into the system, and let us assume for the moment that the two carriers do not interact. In the absence of the tunnelling, the wave function of the pair can be written as a product of the isospin states of each qubit separately. There are four possible configurations: $|0\rangle_e|0\rangle_h$, $|1\rangle_e|1\rangle_h$, $|0\rangle_e|1\rangle_h$, and $|1\rangle_e|0\rangle_h$. Upon the inclusion of tunnelling the qubits will rotate independently, and now the exact wave functions of the system can be written as $|+\rangle_e|+\rangle_h = \frac{1}{2}(|0\rangle_e + |1\rangle_e)(|0\rangle_h + |1\rangle_h)$, and analogously $|-\rangle_e|-\rangle_h$, $|+\rangle_e|-\rangle_h$ and $|-\rangle_e|+\rangle_h$. Thus, the total wave function of the system can be written as a simple product of the electron wave function and the hole wave function, which means that the qubits are not entangled.

Inclusion of the electron-hole Coulomb interaction changes this picture: now the qubits are no longer independent. The Hamiltonian of the system of two interacting qubits in the basis of the quantum-molecular orbitals takes the form:

$$\hat{H} = \sum_i E_i^e c_i^+ c_i + \sum_i E_i^h h_i^+ h_i - \sum_{ijkl} \langle ij|V|kl\rangle c_i^+ h_j^+ h_k c_l, \tag{6.11}$$

where the index $i = +$ or $-$, similarly j, k, and l, and the operators h_i^+ (h_i) create (annihilate) a hole on the orbital i. I construct the basis set out of configurations created by distributing the electron and hole on the molecular orbitals: $\{|+\rangle_e|+\rangle_h,\ |-\rangle_e|-\rangle_h,\ |+\rangle_e|-\rangle_h,\ |-\rangle_e|+\rangle_h.\}$. In a PL experiment only the two first states, i.e., $|+\rangle_e|+\rangle_h$ and $|-\rangle_e|-\rangle_h$ can be addressed optically due to their symmetry; the two remaining states with mixed symmetry are dark. In this basis the Hamiltonian matrix takes the form

$$H = \begin{bmatrix} E_{++} + V_{++++} & V_{++--} & 0 & 0 \\ V_{--++} & E_{--} + V_{----} & 0 & 0 \\ 0 & 0 & E_{+-} + V_{-++-} & V_{-+-+} \\ 0 & 0 & V_{+-+-} & E_{+-} + V_{-++-} \end{bmatrix} \tag{6.12}$$

(details of calculations of the Coulomb matrix elements are given in the paper). This matrix has a block-diagonal form, because the Coulomb interaction mixes only states with the same overall symmetry. In particular, the Hamiltonian matrix does not mix the optically active states with the dark states, and in what follows I will only focus on the top left-hand segment of the matrix,

$$H_A = \begin{bmatrix} E_{++} + V_{++++} & V_{++--} \\ V_{--++} & E_{--} + V_{----} \end{bmatrix}. \tag{6.13}$$

Upon diagonalisation of this simple matrix I obtain the optically active eigenstates of the system of two interacting qubits. If recast in terms of the isospin states, they can be written as

$$|a\rangle = \alpha_1(|0\rangle_e|0\rangle_h + |1\rangle_e|1\rangle_h) + \beta_1(|0\rangle_e|1\rangle_h + |1\rangle_e|0\rangle_h), \tag{6.14}$$

$$|b\rangle = \alpha_4(|0\rangle_e|0\rangle_h + |1\rangle_e|1\rangle_h) + \beta_4(|0\rangle_e|1\rangle_h + |1\rangle_e|0\rangle_h). \tag{6.15}$$

Thus, the states of the pair of interacting qubits cannot be written as simple products of the states of individual qubits, and so the Coulomb electron-hole interaction leads to entanglement of my qubits. The energies corresponding to these two wave functions are composed of orbital and interaction terms. Without interactions the splitting between them would be equal to $E_{++} - E_{--}$, and, for large interdisk distances D, would approach zero. However, due to the off-diagonal matrix element V_{++--}, which changes only weakly with the interdisk distance, the energies of the two optically active states will be split even for large D. This splitting is thus the signature of the entangled states of my qubits. Since both eigenstates, $|a\rangle$ and $|b\rangle$, are optically active, the splitting should be visible in the photoluminescence experiment.

The PL experiment on the InAs/GaAs quantum-disk molecules with varying interdisk distance was performed by the group of Alfred Forchel and Manfred Bayer at Würzburg University. The author of this Thesis, not being involved in the measurements, refers the reader interested in the experimental details to the attached paper. Here let us only state that the splitting of the PL lines due to the recombination of excitons on states $|a\rangle$ and $|b\rangle$ is indeed observed even for the interdisk separations as large as 8 nm. To the best of my knowledge, this is the first successful observation of the PL spectra of an entangled electron-hole pair confined in a double-disk quantum-dot molecule.